

RESEARCH ARTICLE

10.1002/2013JC009396

Horizontal and residual circulations driven by wind stress curl in Tokyo Bay

K. Nakayama^{1,2}, T. Shintani³, K. Shimizu^{4,5}, T. Okada⁶, H. Hinata⁶, and K. Komai¹

Key Points:

- The influence of the wind stress curl on residual currents is clarified
- The deepening of isopycnals is found to be driven by negative wind stress curl
- We proposed to categorize the regimes of nonlinear surface Ekman layer

Correspondence to:

K. Nakayama,
nakayama@mail.kitami-it.ac.jp

Citation:

Nakayama, K., T. Shintani, K. Shimizu, T. Okada, H. Hinata, and K. Komai (2014), Horizontal and residual circulations driven by wind stress curl in Tokyo Bay, *J. Geophys. Res. Oceans*, 119, 1977–1992, doi:10.1002/2013JC009396.

Received 4 SEP 2013

Accepted 24 FEB 2014

Accepted article online 3 MAR 2014

Published online 17 MAR 2014

¹Civil and Environmental Engineering, Kitami Institute of Technology, Kitami, Japan, ²Also at Centre for Water Research, The University of Western Australia, Perth, Australia, ³Civil and Environmental Engineering, Tokyo Metropolitan University, Tokyo, Japan, ⁴The Ocean in the Earth System, Max Planck Institute for Meteorology, Hamburg, Germany, ⁵Now at CSIRO, Marine and Atmospheric Research, Perth, Australia, ⁶Coastal, Marine and Disaster Prevention Department, National Institute for Land and Infrastructure Management, Yokosuka, Japan

Abstract This study investigates the horizontal and residual circulations in Tokyo Bay using field observations, numerical simulations, and theoretical analysis. Numerical simulations show that the observed deepening of isopycnals and associated anticyclonic horizontal circulation in the bay head are mainly driven by negative wind stress curl. The effects of river discharge, surface heat fluxes, and tides are found to be small. Under strong wind events, the wind stress curl over the bay head can be large enough to make the surface Ekman layer strongly nonlinear. Theoretical and numerical analyses show that, under large negative wind stress curl, the nonlinearity tends to induce positive pumping velocity (at the base of the surface mixed layer) that counteracts the Ekman pumping; however, the typical duration of wind events in the bay head is not long enough to induce positive pumping under negative wind stress curl. These results and historical wind data suggest that the average horizontal circulation and residual circulation immediately below the surface mixed layer in Tokyo Bay are, respectively, cyclonic and convergent in summer but anticyclonic and divergent in winter.

1. Introduction

Understanding the transport of particulate matter by horizontal and residual circulations is important for effective water resource management. For example, in Tokyo Bay, Japan, organic matter and nutrients from rivers settle onto the seabed in lower energy environments [Guo and Yanagi, 1996], leading to a deterioration in the water quality of the bay [Okada et al., 2011]. The average depth at the bay head is about 15 m and the settling speed of organic matter is estimated to be 0.4 m a day [Horiguchi and Nakata, 1995], so it takes about a month for organic matter to settle. This means that long-term mass transport due to horizontal and residual circulations will be particularly influential in mass accumulation [Guo and Yanagi, 1998], which occurs at a rate of 0.3 g cm⁻² a year [Matsumoto and Saito, 1984]. The residual current due to baroclinic effects and winds has the greatest influence on long-term transport of organic matter around the bay head, where the production of organic matter predominantly occurs [Nakayama et al., 2005; Okada et al., 2011]. However, the effects of wind stress curl on horizontal and residual circulations in Tokyo Bay have not been adequately investigated.

Previous studies on horizontal circulation in Tokyo Bay focused on the effects of internal waves and estuarine circulation. Sugino-hara [1974] showed that, under northerly winds, internal Kelvin waves excited by upwelling along the eastern coast travel around the bay and break on the western coast due to collision with downwelling. Suzuki and Matsuyama [2000] used this theory to show that anticyclonic horizontal circulation occurs as a result of a compensation current in the upper layer due to the internal Kelvin wave. Tanaka [2001] applied the theory of Fujiwara et al. [1997] to Tokyo Bay, and further showed that anticyclonic horizontal circulation in the thermocline around the bay head is due to estuarine circulation. Northerly winds have also been found to enhance estuarine circulation and the anticyclonic horizontal circulation. However, Nakayama et al. [2005] showed that downwelling occurs in conjunction with convergence around the head of Tokyo Bay, and Fujiwara et al.'s theory cannot explain the anticyclonic horizontal circulation in Tokyo Bay.

In other semienclosed bays and lakes, surface heat fluxes and wind stress curl are important driving forces of horizontal circulation. Cooling and river inflow cause anticyclonic horizontal circulation in Ise Bay

[Fujiwara, 2003], whereas heating and barolinicity can be the major forcing for cyclonic circulation in summer in Lake Biwa [Endoh, 1986] and Lake Michigan [Schwab and Beletsky, 2003]. Spatially variable winds are one of the major, if not dominant, driving forces in many bays and lakes, such as the Adriatic Sea [Zavatarelli et al., 2002], Lake Michigan in winter [Schwab and Beletsky, 2003], Lake Kinneret [Laval et al., 2003], and Lake Biwa [Shimizu et al., 2007; Akitomo et al., 2009]. Wind stress curl can be large for water bodies surrounded by a complex terrain [Rueda et al., 2005].

If wind stress curl is one of the major driving forces, Ekman pumping is important for the excitation of horizontal circulation as well as residual circulation. Under constant positive wind stress curl, for example, divergent Ekman transport induces positive Ekman pumping and stretching of the water column, which spins up cyclonic horizontal circulation through the conservation of potential vorticity [Pedlosky, 1979; Gill, 1982]. As shown later in this study, the magnitude of wind stress curl can be large enough to make the Ekman layer strongly nonlinear in bays surrounded by complex terrain. Stern [1965], Thomas and Rhines [2002], and Pedlosky [2008] obtained weakly nonlinear corrections to the linear Ekman layer solution. It appears that a strongly nonlinear Ekman layer has not been considered in an oceanic context, though strongly nonlinear rotating boundary layers have been investigated in a closely related von Kármán swirling flow problem [e.g., Rogers and Lance, 1960; Benton et al., 1964; Zandbergen and Dijkstra, 1987]. In addition to the spin-up of horizontal circulation, to close the circuit of Ekman transport, and to satisfy the conservation of mass, Ekman and nonlinear transport also induces three-dimensional residual flow [Greenspan, 1968]. This flow is especially strong within and immediately below the surface Ekman layer, and the flow persists even after the completion of spin-up. In shallow bays, the surface Ekman layer can occupy a significant portion of the water column, and such residual circulation could be important for long-term basin-wide mass transport.

This study aims to show that wind stress curl is the major driving force of horizontal circulation in Tokyo Bay, and to investigate potential roles of strongly nonlinear surface Ekman layer in driving residual circulation. To achieve the first aim, we use a combination of field observations and numerical modeling. Field observations suggest a coincidence of negative wind stress curl and the depression of isopycnals in the bay head. We conduct numerical modeling to confirm that wind stress curl is the major driving force, and the effects of river discharge, surface heat fluxes, and tides are small. To achieve the second aim, we carry out theoretical analysis and numerical modeling of a strongly nonlinear surface Ekman layer. Both theoretical and numerical solutions show that, in contrast to existing perturbation solutions, vertical velocity at the base of the surface mixed layer (hereafter referred to as pumping velocity) becomes more positive under strongly negative wind stress curl, as the centrifugal force dominates the Coriolis force.

This paper is organized as follows. We briefly introduce the study site, Tokyo Bay, in section 2. We present the results of field experiments in section 3, and use a numerical computational model, FANTOM3D [Maruya et al., 2010; Nakayama et al., 2012; Nakamoto et al., 2013] to understand the results of field experiments in section 4. In section 5, we investigate the role of nonlinearity in a surface Ekman layer both theoretically and numerically. The results of this study based on a short timescale (a few days) are put into context of long-term mass transport in section 6 followed by conclusions.

2. Study Site

Tokyo Bay has a width and length of about 15 and 60 km, respectively (Figure 1). The average depth of the bay changes sharply from a few hundreds of meters at the bay mouth to 15 m at the bay head. Tokyo Bay is stratified throughout the year due to freshwater input from rivers and intrusion of saline sea water from the Pacific Ocean. There are four predominant tides in Tokyo Bay, M2, S2, K1, and O1. M2 is the most significant of the four and has an amplitude of about 0.4 m at the bay mouth. During spring tides, the maximum velocity around the bay mouth is greater than 1 m s^{-1} . Mixing associated with this strong current makes stratification around the bay head approximately linear, but weaker mixing, heating in spring and summer, and freshwater input cause a weak pycnocline at a depth of about 8 m around the shallow bay head. The stratification enables winds to cause larger velocities near the surface because the effective water depth is shallower due to the suppression of vertical momentum transfer. Around the bay head, the influence of tides on currents is small relative to that of winds.

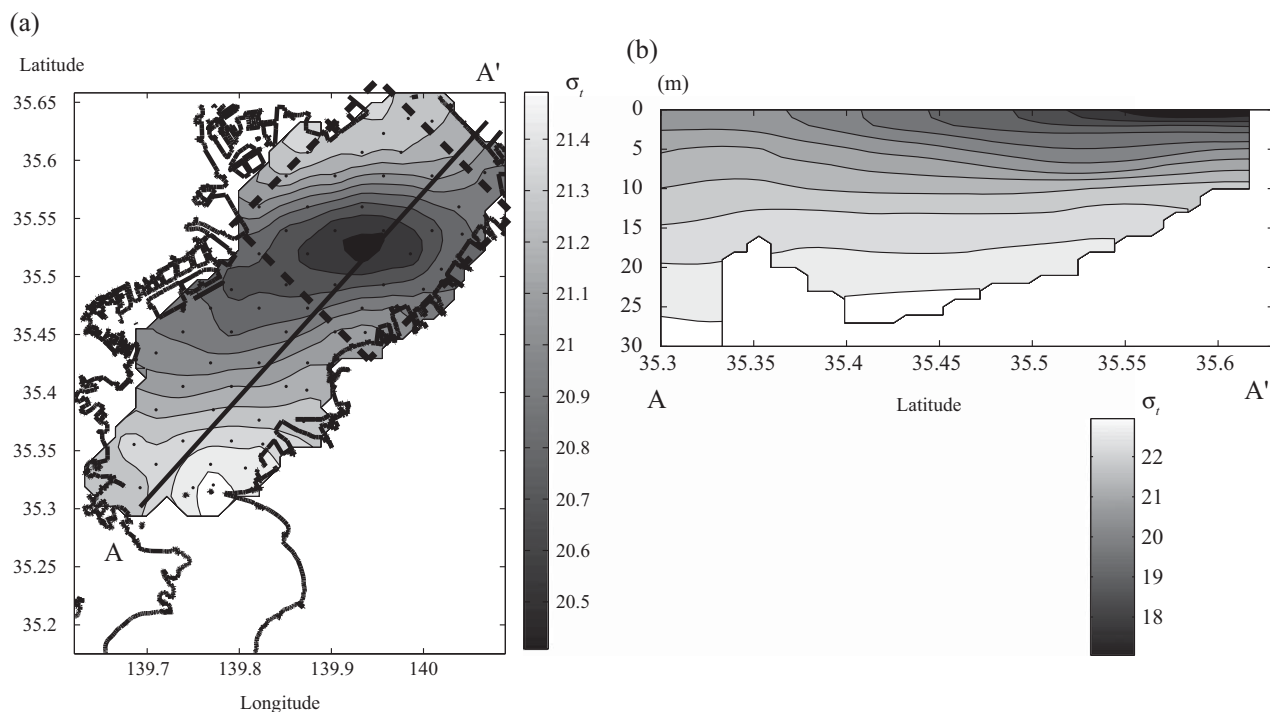


Figure 1. Field observations on 10 August 2001. Salinity and water temperature were observed at 65 stations shown by dots. (a) Horizontal distribution of σ_t at a depth of 8 m. (b) Vertical distribution of σ_t along A-A'.

3. Observations

3.1. Field Experiments and Data Processing

Three field experiments were carried out to measure salinities and water temperatures in Tokyo Bay. The most detailed data set was collected on 10 August 2001 by lowering AST-500 sensors (Alec Electronic Corporation) at 65 stations, with a spatial interval of about 3.5 km and a vertical interval of 0.1 m (Figure 1) [Kasuya *et al.*, 2004; Nakayama *et al.*, 2005]. During the field experiment, the tide was at its neap phase with an amplitude of 0.6 m. The entire study area was divided into eight sections, and one ship was used in each section so that field experiments could be completed quasimultaneously within 5 h during daylight hours. Two other experiments were carried out on 30 October 2002 and 18 December 2002 with similar methodology but coarser horizontal and vertical resolutions (21 stations with a 0.5 m vertical interval; Figures 2c and 2d).

Wind fields around Tokyo Bay were estimated using nine land-based meteorological observation stations of the Automated Meteorological Data Acquisition System (AMeDAS System), since topography around the bay induces shear and curl in the wind field. Since the observed wind speed at a height of 10 m over Tokyo Bay has been found to be about twice that measured at a height of 10 m on land [Nakayama *et al.*, 2005, 2010; Satoh *et al.*, 2012], we doubled the wind speeds observed by the AMeDAS system and then interpolated the wind vectors using an exponential weighting function. To validate this technique for estimating the wind fields, we compared the observed wind vectors at a station to the wind vectors interpolated without using the data from the station. The high correlation between the observed and estimated wind vectors (not shown) indicates the validity of this interpolation technique. The average wind curl shown below was computed by averaging wind curl in the square enclosed by broken lines in Figure 1a.

3.2. Depression of Isopycnals and Wind Curl

On 10 August 2001, we observed a round-shaped depression of the isopycnals with a diameter of about 10 km (Figure 1), suggesting the convergence of the surface water into the center of the bay head. The spatial average of wind curl around the bay head at 9:00 as well as its 1 day average was $-2 \times 10^{-4} \text{ s}^{-1}$ (Figure 3d). The depression of isopycnals was weaker on 30 October 2002 and 18 December 2002 (Figure 2). On 10

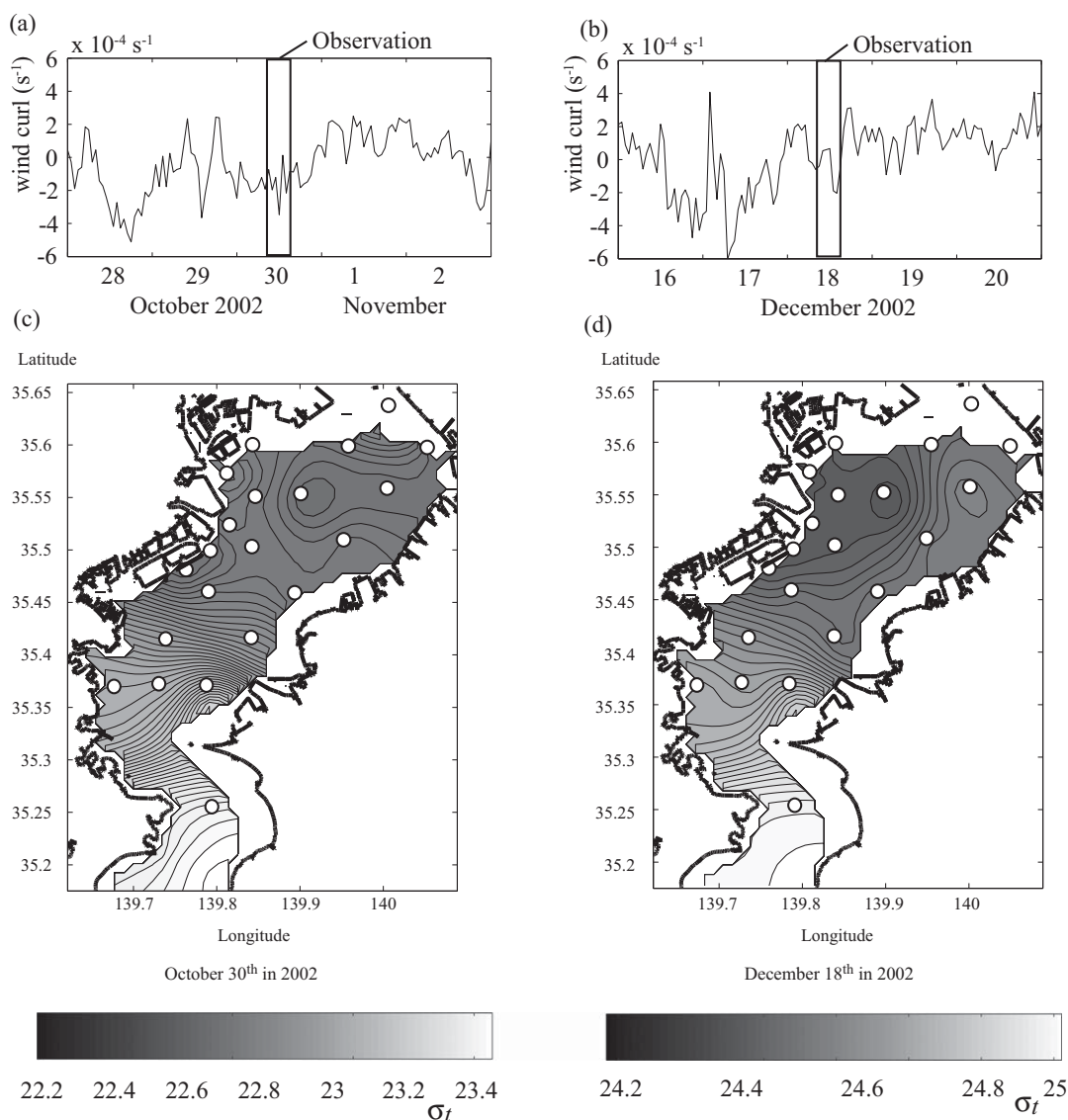


Figure 2. Field observations on (left) 28 October 2002 to 1 November 2002 and (right) 16–20 December 2002. (a and b) Low-pass filtered (with a cutoff period of 24 h) wind curl and (c and d) horizontal distribution of σ_t at a depth of 10 m.

October 2002, wind curl had a magnitude similar to 10 August 2001, but it was positive on the previous day. This probably led to smaller depression of the isopycnals. The wind curl was small and negative on 18 December 2002 and the depression of the isopycnals was not as evident. These field experiments suggest that the observed depression of the isopycnals was probably driven by negative wind curl and maintained by anticyclonic horizontal circulation, and that the depression is sensitive to wind curl and its history. In the next section, numerical simulations are used to test these hypotheses.

4. Numerical Solutions

4.1. Model Description and Configuration

A three-dimensional nonhydrostatic model, FANTOM3D, was used to clarify the role of negative wind curl on the occurrence of the depression of the isopycnals due to Ekman transport [Maruya *et al.*, 2010; Nakayama *et al.*, 2012; Nakamoto *et al.*, 2013] and the associated anticyclonic horizontal circulation. FANTOM3D is an object-oriented programming model for the analysis of environmental fluid mechanics. Parallel computing was employed and the computational domain divided into four subdomains. To simulate

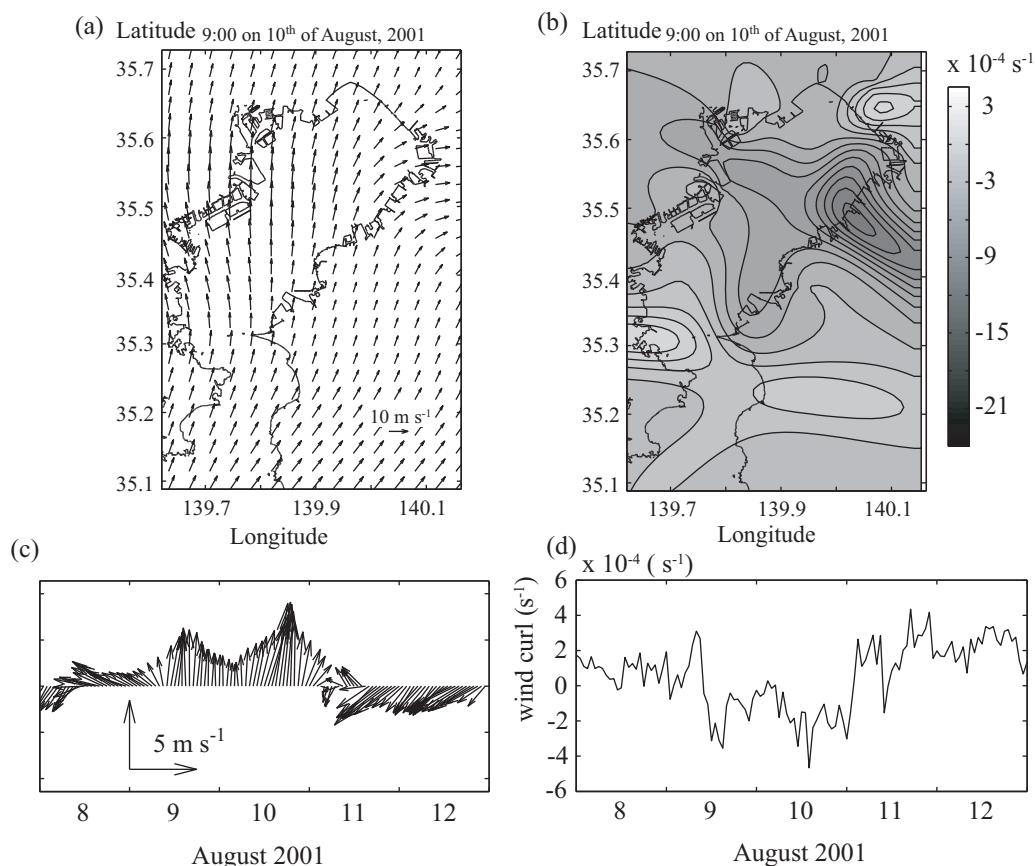


Figure 3. Wind field over Tokyo Bay around 10 August 2001. (a) Wind vector and (b) wind curl at a height of 10 m on land at 9:00 on 10 August 2001. (c) Wind vector and (d) wind curl on 8–12 August 2001.

topographic effects accurately and to prevent numerical diffusion, the z coordinate system was employed [Nakayama, 2006; Simanjuntak et al., 2009; Nakayama and Imberger, 2010]. The vertical mixing scheme was based on large-eddy simulation [Orlandi, 2000], the advection scheme for momentum and scalar was ULTIMATE-QUICKEST [Leonard, 1991] while for subgrid-scale turbulent kinetic energy a first-order upwind scheme was used. The computational domain had $60 \times 45 \times 50$ grid points with the grid intervals of $1 \text{ km} \times 1 \text{ km} \times 1 \text{ m}$. The time step was 60 s. The model was forced with winds, river discharge, surface heat fluxes, and tides.

In numerical simulations, we focused on 10 August 2001, because more detailed data were available and larger depression of the isopycnals was observed. The model was initialized with horizontally uniform stratification taken from the measured density profile at 15 km from the bay head on 10 August 2001. The wind forcing was given based on the interpolated wind field described in the previous section. Surface elevations at the open boundary were forced by the observed tide level at the Mera station, which is located at $34^{\circ}55'N$ and $139^{\circ}50'E$ about 70 km south of the bay head shown at the bottom of Figure 1. Observed discharges from the four main rivers, Edo, Ara, Tama, and Tsurumi Rivers, were taken into account (Figure 4a). Short and long wave radiations and sensible and latent heat fluxes were calculated from air temperature, humidity, cloud cover, net radiation, and wind speed at the Mera station using the bulk formulae by Kondo [1975].

4.2. Effects of Wind Curl, River Discharge, Surface Heat Fluxes, and Tides on Horizontal Circulation

The simulation was first run from 1 August to 30 August including all the forcing. The results reproduced the observed depression of the isopycnals well (compare Figures 1a and 4b), even though horizontally

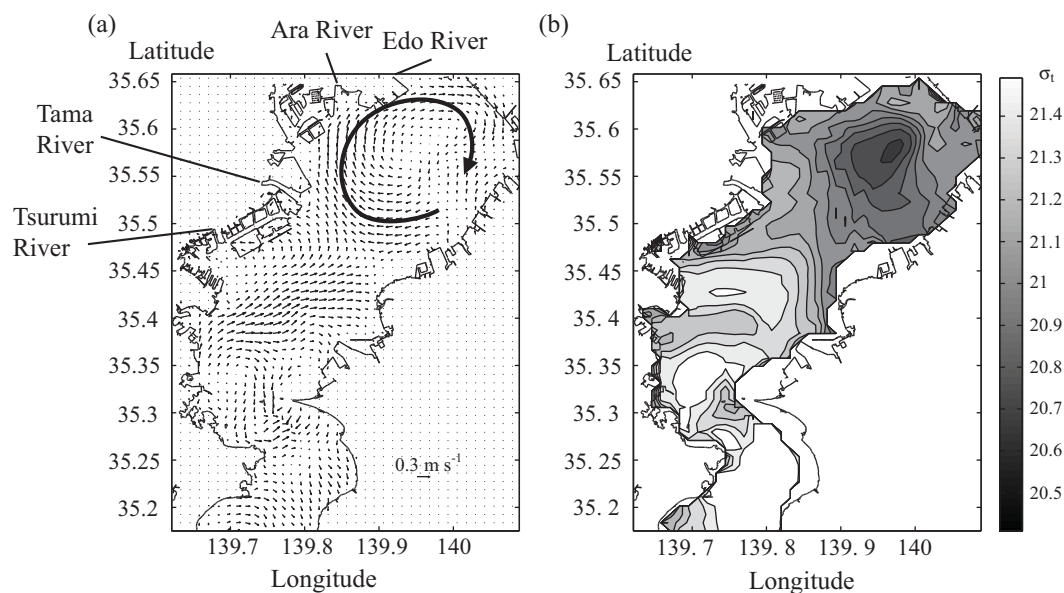


Figure 4. Numerical simulation results for Case 1 at 9:00 on 10 August 2001. (a) Computed average velocity vector at a depth of 5 m. (b) Computed σ_t at a depth of 8 m.

uniform stratification was used as an initial condition. The depression was associated with anticyclonic horizontal circulation around the bay head (Figure 4a).

To investigate the relative importance of negative wind curl, river discharge, surface heat fluxes, and tides, we carried out further simulations for the same period (Table 1). We varied forcing in these simulations, but kept the other model configurations the same. In the following, the computational result shown in Figure 4b is referred to as Case 1. Surface heat fluxes and river discharge were excluded in Cases 2 and 3, respectively. In Case 4, we used a time series of spatially averaged winds. The effect of tides was small and the results are not shown in this paper.

For the cases without river discharge or surface heat fluxes (Cases 2 and 3), negative wind curl clearly caused a round-shaped depression of the isopycnals with a diameter of about 10 km in the center of the bay head (Figures 5a and 5b). River discharge slightly increased isopycnal depression, but surface heat fluxes had no marked effect. Comparison of Cases 1 and 4 (Figures 4b and 5c) showed that negative wind curl was essential to induce the depression. Thus, the simulations revealed that the depression of the isopycnals observed on 10 August 2001 was caused mainly by surface water convergence driven by negative wind curl.

4.3. Effects of Magnitude and Duration of Wind Curl on Divergence

To further investigate the effect of the magnitude and duration of wind curl on the depression of isopycnals, we investigated the transient response to wind forcing with constant wind curl over the head of Tokyo Bay (Figure 6). The simulations were started as described earlier, and wind forcing was kept constant in time. Case A01 corresponds to the 1 day mean wind curl on 10 August 2001 ($-2 \times 10^{-4} \text{ s}^{-1}$), and wind curl with larger but realistic magnitudes are considered here (Table 2; statistics of wind curl over Tokyo Bay will be shown in section 6). To evaluate the doming and depression of the isopycnals, we calculated the spatial average of the vertical velocity in the upper 8 m within 5 km from the center of the wind curl. Since the vertical velocity fields were smooth over this region (Figure 6c), conclusions drawn from the averaged vertical velocity are insensitive to the averaging method.

In Case A01, the maximum negative vertical velocity occurred 7 h after the onset of the wind forcing, followed by damped oscillations (Figure 7a). The maximum negative vertical velocity increased with the magnitude of negative wind curl (Figures 6b and 7a). The inertial period is about $2\pi/f = 17.6$ h, which agrees with the period of oscillation seen in Cases A01 to A04. These features are expected from Ekman pumping and a transient response of the linear Ekman layer. Interestingly, however, vertical velocity became positive after around 20 h if the magnitude of negative wind curl was large (Figure 7a). This suggests that

Table 1. Numerical Simulation Cases to Investigate the Relative Effects of Different Forcing

	Wind	Rivers	Heating/Cooling
Case 1	Negative curl	Included	Included
Case 2	Negative curl	Included	Not included
Case 3	Negative curl	Not included	Included
Case 4	Homogeneous wind field	Included	Included

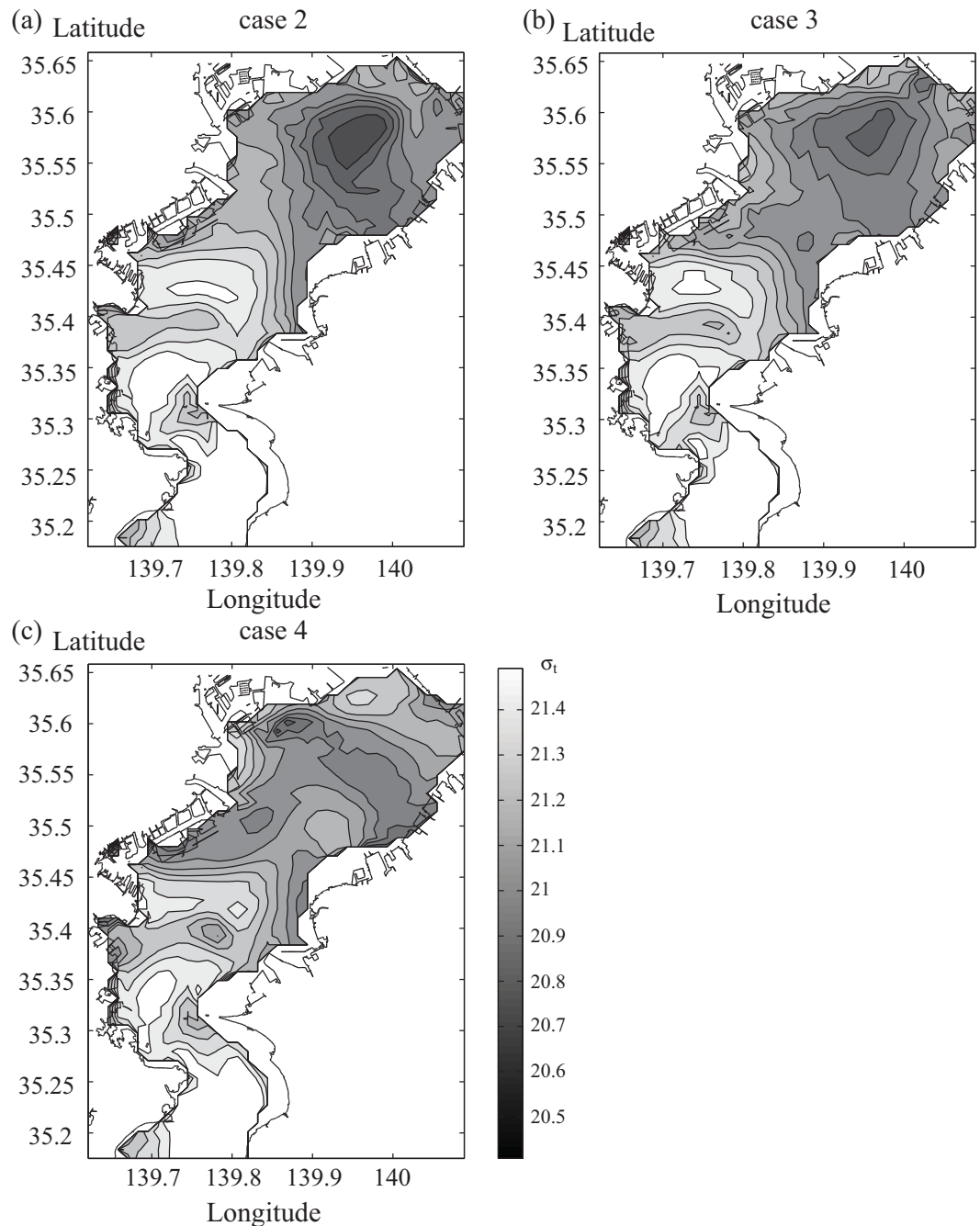


Figure 5. Numerical simulation results for Cases 2–4. Computed σ_t at a depth of 8 m is shown. (a) Case 2: Surface heat fluxes are excluded. (b) Case 3: River inflow is excluded. (c) Case 4: a homogeneous wind field with river inflow and surface heat fluxes.

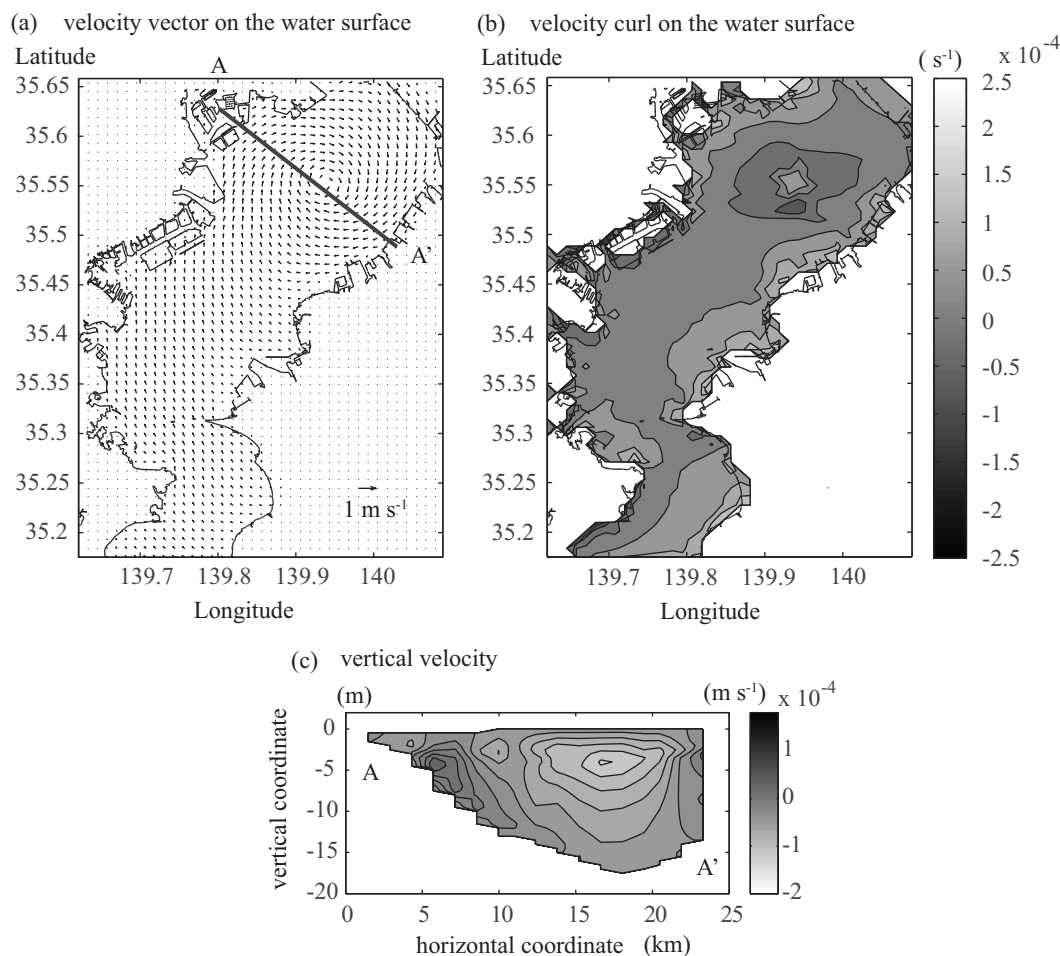


Figure 6. Simulation results at 6 h after the beginning of the simulation in Case A04. (a) Velocity vector at water surface, (b) velocity curl on the water surface, and (c) vertical velocity in the A-A' vertical cross section.

mechanisms other than Ekman pumping induce positive vertical velocity even under negative wind curl. On the other hand, positive wind curl always caused positive vertical velocity (Figure 7b), and its magnitude increased with increasing positive wind curl.

Table 2. Numerical Simulation Cases to Investigate the Effects of Wind Curl in Tokyo Bay

	Mean Wind Curl in Bay Head (s^{-1})	Coriolis
Case A01	-2×10^{-4}	Included
Case A02	-4×10^{-4}	Included
Case A03	-6×10^{-4}	Included
Case A04	-8×10^{-4}	Included
Case A05	2×10^{-4}	Included
Case A06	4×10^{-4}	Included
Case A07	6×10^{-4}	Included
Case A08	8×10^{-4}	Included
Case A09	-2×10^{-4}	Not included
Case A10	-4×10^{-4}	Not included
Case A11	-6×10^{-4}	Not included
Case A12	-8×10^{-4}	Not included
Case A13	2×10^{-4}	Not included
Case A14	4×10^{-4}	Not included
Case A15	6×10^{-4}	Not included
Case A16	8×10^{-4}	Not included

To see what causes positive Ekman pumping under strongly negative wind curl, we carried out additional model runs (Cases A09 to A16) excluding the Coriolis effect (Figures 7c and 7d). These cases showed only positive vertical velocity irrespective of the sign of the wind curl, and that the vertical velocity increased with the magnitude of wind curl. This can be understood as follows. Viscosity transfers the momentum given by wind stress downward and drives horizontal current in the Ekman layer. At the same time, the centrifugal force tends to push the water parcel outward. Since the horizontal current weakens with increasing depth due to viscosity, the centrifugal force

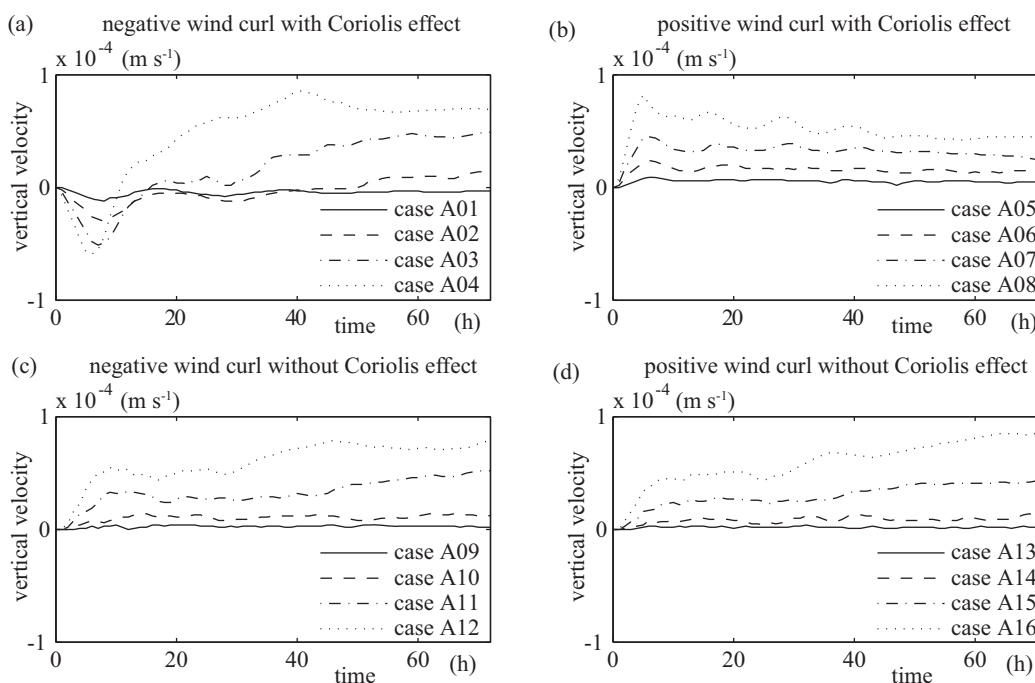


Figure 7. Vertical velocity averaged within 5 km from the center of the wind curl (Figure 6) and in the upper 8 m. (a) Cases A01 to A04: negative wind curl with Coriolis effect. (b) Cases A05 to A08: positive wind curl with Coriolis effect. (c) Cases A09 to A12: negative wind curl without Coriolis effect. (d) Cases A13 to A16: positive wind curl without Coriolis effect.

is stronger near the surface. This induces stronger radial flow near the surface, and in turn upward flow to conserve mass, in the absence of the Coriolis force. In the presence of the Coriolis force, the vertical velocity in the surface water, or pumping velocity at the base of mixed layer, is determined by a balance between Ekman and nonlinear pumping. Since the pumping velocity drives three-dimensional residual circulation in the surface water (Figures 6b and 6c), the nonlinear pumping can be important not only for driving horizontal circulation but also for driving residual circulation.

The results here show that the wind stress curl over Tokyo Bay can be large enough to make the Ekman layer nonlinear, and that the effects of nonlinearity are different from previous perturbation solutions [Thomas and Rhines, 2002; Pedlosky, 2008], which predict that nonlinearity makes the pumping velocity more negative. Therefore, we further investigate the interplay between the Coriolis and nonlinear effects in a nonlinear Ekman layer in idealized settings in the next section.

5. Nonlinear Ekman Layer

5.1. Theoretical Analysis

To understand the effects of centrifugal forces on pumping velocity conceptually, we consider a nonlinear Ekman layer in a simple setting, following previous studies on the von Kármán swirling flow problem [e.g., Rogers and Lance, 1960; Benton et al., 1964; Zandbergen and Dijkstra, 1987]. We consider a horizontally infinite homogeneous fluid in cylindrical coordinates (r, θ, z) , and assume idealized wind stress $\tau = (\tau_r, \tau_\theta) = (0, \rho_0 T r)$ and eddy viscosity $\nu = \nu(z)$, where ρ_0 is the reference density and T is half the wind stress curl (note $\rho_0^{-1} \nabla \times \tau = 2T$). Due to the form of the forcing, the problem does not depend on θ . Writing velocity components in (r, θ, z) as (u, v, w) and using dynamic pressure p , the Reynolds-averaged Navier-Stokes equations for a thin Ekman layer become

$$\frac{\partial u}{\partial t} + u \frac{\partial u}{\partial r} + w \frac{\partial u}{\partial z} - \frac{v^2}{r} = -\frac{1}{\rho_0} \frac{\partial p}{\partial r} + f v + \frac{\partial}{\partial z} \left(\nu \frac{\partial u}{\partial z} \right), \quad (1a)$$

$$\frac{\partial v}{\partial t} + u \frac{\partial v}{\partial r} + w \frac{\partial v}{\partial z} + \frac{uv}{r} = -fu + \frac{\partial}{\partial z} \left(\nu \frac{\partial v}{\partial z} \right), \quad (1b)$$

$$\frac{\partial w}{\partial t} + u \frac{\partial w}{\partial r} + w \frac{\partial w}{\partial z} = -\frac{1}{\rho_0} \frac{\partial p}{\partial z} + \frac{\partial}{\partial z} \left(\nu \frac{\partial w}{\partial z} \right), \quad (1c)$$

$$\frac{1}{r} \frac{\partial}{\partial r} (ru) + \frac{\partial w}{\partial z} = 0, \quad (1d)$$

where f is the Coriolis parameter. Following *Benton et al.* [1964], we assume a solution of the form:

$$(u, v, w)(r, z, t) = (rU(z, t), rV(z, t), W(z, t)), p(r, z, t) = P(z, t) + \frac{1}{2}G(t)r^2. \quad (2)$$

Substituting (2) into (1) and using prime to denote derivative with respect to z , (1) becomes

$$\frac{\partial U}{\partial t} + U^2 + V^2 + WW' = (f + 2V)V + (\nu U')' - G, \quad (3a)$$

$$\frac{\partial V}{\partial t} + WV' = -(f + 2V)U + (\nu V')', \quad (3b)$$

$$\frac{\partial W}{\partial t} + WW' = -\frac{1}{\rho_0} P' + (\nu W')', \quad (3c)$$

$$2U + W' = 0. \quad (3d)$$

Note that the curl of horizontal velocity is

$$\zeta = \frac{1}{r} \frac{\partial}{\partial r} (rv) = 2V. \quad (4)$$

Boundary conditions at the surface were continuity of stress and zero vertical velocity. In this study, we assumed a slip boundary condition at the base of the mixed layer to include idealized effects of stratification:

$$\nu U' = 0, \nu V' = T, W = 0 \text{ at } z = 0, \quad (5a)$$

$$\nu U' = \nu V' = 0 \text{ at } z = -h, \quad (5b)$$

where h is the mixed layer depth. Now, the problem is reduced to (z, t) . In this study, we consider simpler cases of steady state with $G = 0$ and constant ν . Then, (3a), (3b), and (3d) can be solved for (U, V) , and (3c) determines the pressure P .

The linear solution to (3) for a very thick mixed layer ($h \rightarrow \infty$) is the well-known Ekman layer solution. The Ekman pumping velocity w_E is $2T/f$ regardless of the flow structure in the Ekman layer, and the amplitude of (U, V) at the surface is $T/\sqrt{2\nu f}$. Previous studies extended the linear solution toward larger magnitudes of wind stress by the perturbation method [*Brink, 1997; Hart, 2000; Thomas and Rhines, 2002; Pedlosky, 2008*]. We numerically integrated (4a), (4b), and (4d) in order to investigate the dynamics of a strongly nonlinear Ekman layer.

Obtaining numerical steady solutions to (3) are not trivial because multiple solutions exist, as in the von Kármán swirling flow problem [*Zandbergen and Dijkstra, 1987*], in which the Coriolis term in (3) is not considered and upper boundary conditions are given by azimuthal velocity instead of stress. Multiple solutions to (3) are not necessarily physically plausible, and we need to find solutions that are physically plausible and that correspond to the simulation results in Tokyo Bay. In this study, we first solved (3a)–(3c) by

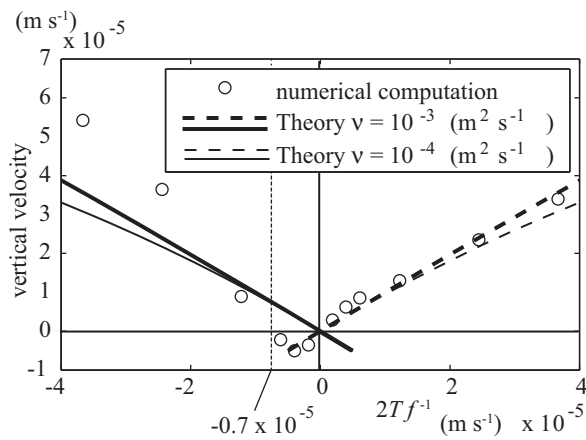


Figure 8. Relationship between wind stress curl divided by the Coriolis parameter (Ekman pumping velocity for the linear Ekman layer) and total pumping velocity for strongly nonlinear Ekman layers. Circles indicate numerical solutions. Thin and thick lines indicate theoretical solutions for $\nu = 10^{-4}$ and $10^{-3} \text{ m}^2 \text{ s}^{-1}$, respectively. Dashed and solid lines indicate the first and second branches, respectively.

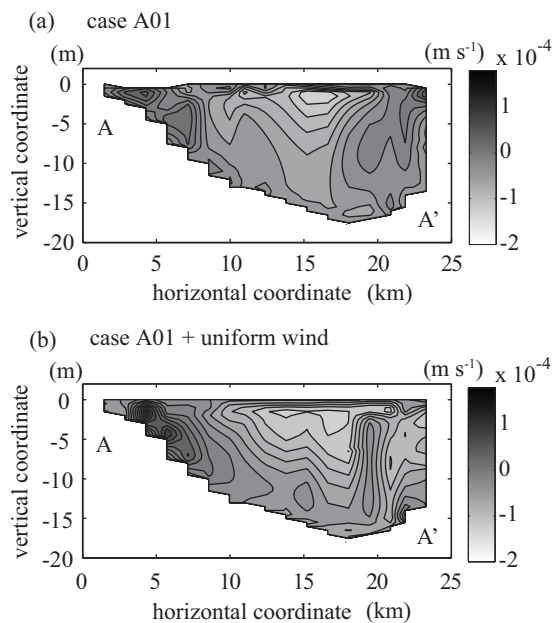


Figure 9. Vertical velocity in the A-A' vertical cross section in Figure 6a at 6 h after the beginning of the simulations. (a) Case A01 and (b) winds as in Case A01 plus uniform wind with the magnitude of 1.5 m s^{-1} .

obtained by starting from positive and negative wind stress curl are referred to as the first and second branches, respectively. The first branch corresponds to a typical Ekman layer modified by nonlinearity (as long as the mixed layer is thick enough). Perturbation solutions obtained in previous studies [e.g., Thomas and Rhines, 2002; Pedlosky, 2008] correspond to this branch. The second branch is symmetric to the first branch (Figure 8) because, if (U, V, W) is a solution to (3) for forcing T , $(U, -f - V, W)$ is a solution for forcing $-T$. The second branch is a strongly nonlinear branch because the solution of the form $(U, -f - V, W)$ exists due to the nonlinear terms in (3) even under weak forcing. The azimuthal velocity gradient $-f - V$ means that there is a jump in horizontal velocity at the base of the mixed layer, which would cause stronger mixing there. Note that the theoretical solutions to (3) do not show when a transition between branches occurs.

discretizing the equation using the second-order finite difference method in the vertical with a grid size of 0.01 m and using an implicit time-stepping scheme with a time step of $T_i/8$ (T_i is the inertial period). We used $h = 4 \text{ m}$ and considered a range of $\nu = 1.0 \times 10^{-5} - 1.0 \times 10^{-3} \text{ m}^2 \text{ s}^{-1}$. We first solved the discretized equations from the rest by suddenly imposing positive and negative wind stress curl of large magnitude ($2T/f = \pm 1 - 3 \times 10^{-4}$), to obtain two initial solutions. To obtain solutions for wind stress curl of smaller magnitudes, we employed a method somewhat similar to Rogers and Lance [1960]; we made the magnitude of wind stress curl slightly smaller (by $2T/f = \pm 5 \times 10^{-6}$), used the previously obtained initial solutions to (3) as an initial condition, and solved the equations. We repeated this process to obtain two solution branches for a range of wind stress curl. The above procedure enabled us to obtain two initial solutions under conditions similar to the numerical simulations. Although which branch a numerical steady solution belongs to is sensitive to computational conditions (numerical scheme, initial condition, history of forcing, etc.) in general, the two branches obtained using the above procedure were relatively robust.

The results show two branches, both of which induce positive pumping, except for under weak forcing (Figure 8). The branches

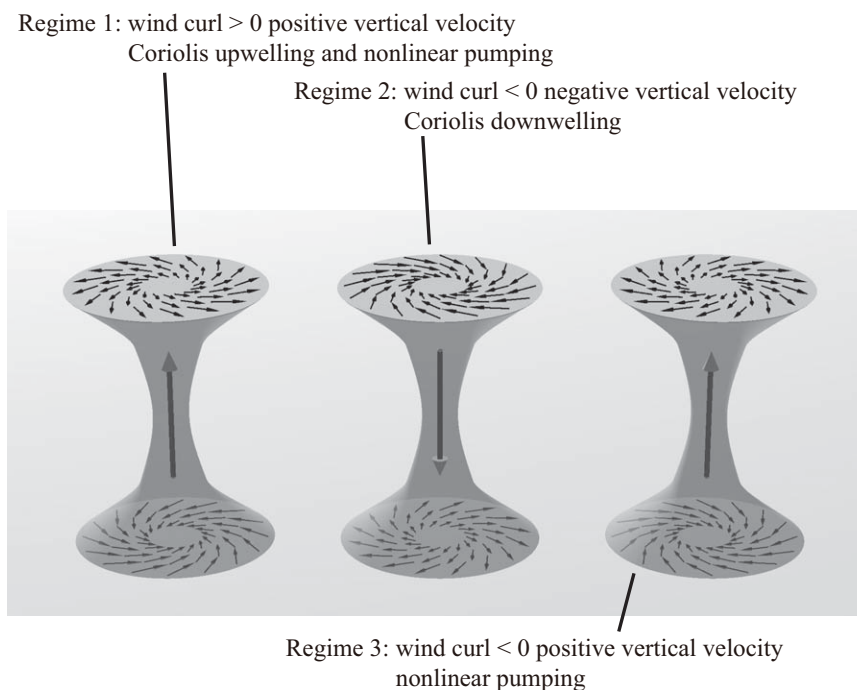


Figure 10. Schematic diagram of regimes of nonlinear Ekman layers. Regime 1 ($w_{E0} = 2T/f > 0$)—cyclonic circulation with upwelling due to Coriolis upwelling and nonlinear pumping; Regime 2 ($-0.7 \times 10^{-5} \text{ m s}^{-1} < w_{E0} = 2T/f < 0$)—anticyclonic circulation with downwelling due to Coriolis downwelling; and Regime 3 ($w_{E0} = 2T/f < -0.7 \times 10^{-5} \text{ m s}^{-1}$)—anticyclonic circulation with conditional upwelling due to nonlinear pumping.

5.2. Comparison With 3-D Model

To investigate whether the theoretical solutions to (3) are physically plausible and when a transition between the branches occurs, we ran FANTOM3D under conditions comparable to the theoretical solutions. We idealized the head of Tokyo Bay as a cylinder of 20 km diameter and 20 m height. The model was forced with spatially uniform wind stress curl shown in Table 3, and the rest of the conditions including initial stratification were the same as that used in section 4. The surface Ekman layer thickness was around 4 m in this condition.

For comparison, we wanted to generalize the results by using nondimensional variables such as the Rossby number (a typical ratio of nonlinear to Coriolis terms in (4a) and (4b)) $Ro = \zeta/f$ [Brink, 1997] or $Ro = 2T/f\sqrt{2\nu f}$ (similar to Pedlosky [2008]), and Ekman pumping velocity normalized by the linear solution $w_{E0}/(2T)$. However, for a surface Ekman layer, the Rossby number is not robust because the definition involves either relative curl or eddy viscosity, which greatly depends on the vertical grid resolution or parameterization of

turbulence in typical simulation conditions at a bay scale. As a compromise, we decided to use Ekman pumping velocity in the linear limit $w_{E0} = 2T/f$ as a measure of the strength of forcing and compare it against actual (nonlinear) pumping velocity at the base of the surface Ekman layer. We found this relationship less sensitive to the choice of vertical grid resolution and parameterization of eddy viscosity. For example, changing ν from 10^{-5} to $10^{-3} \text{ m}^2 \text{ s}^{-1}$ caused about 40% change in w_{E0} (Figure 8).

The numerical solutions corresponded to the two branches of the theoretical solutions (Figure 8). In the case of negative wind stress curl, the agreement was not as good, but still reasonable considering the simplifications used to obtain the theoretical solutions. A possible source of discrepancy is mixing at the base of the mixed layer. For negative wind

Table 3. Numerical Simulation Cases for Comparison With Theoretical Solutions of a Strongly Nonlinear Ekman Layer

	Wind Stress Curl (m s^{-2})
Case B01	-18.2×10^{-10}
Case B02	-12.1×10^{-10}
Case B03	-6.06×10^{-10}
Case B04	-3.03×10^{-10}
Case B05	1.97×10^{-10}
Case B06	-0.91×10^{-10}
Case B07	0.91×10^{-10}
Case B08	1.97×10^{-10}
Case B09	3.03×10^{-10}
Case B10	6.06×10^{-10}
Case B11	12.1×10^{-10}
Case B12	18.2×10^{-10}

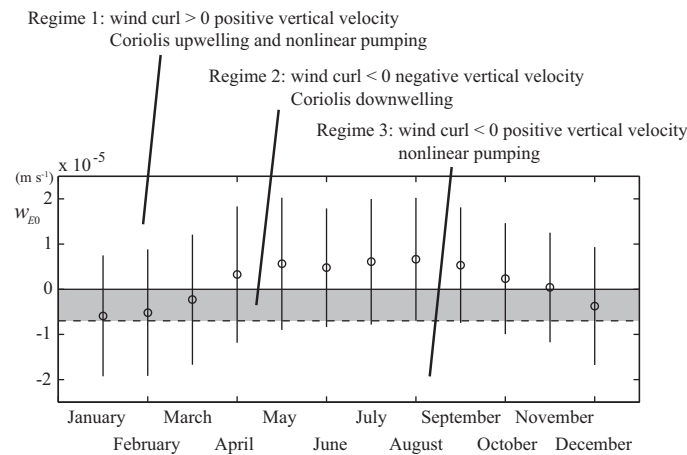


Figure 11. Monthly statistics for $w_{E0} = 2T/f$ over the head of Tokyo Bay. Circles indicate the monthly average and bars the standard deviation. Broken lines indicate the threshold between the regimes of nonlinear Ekman layers.

stress curl, the pumping velocity was negative when the magnitude of stress curl was small, but showed a transition from the first to the second branch around $w_{E0} = -0.7 \times 10^{-5} \text{ m s}^{-1}$.

Note that the results here were not very sensitive to adding spatially uniform wind stress. This is clear for the theoretical solutions because spatially uniform wind stress does not affect wind stress curl and the solution is independent of the origin of horizontal coordinates. For numerical solutions, the existence of horizontal boundary complicates the situation, but we confirmed that spatially uniform wind stress did not

change the results, at least qualitatively (Figure 9). Therefore, the above analysis can be applied to more realistic wind stress, which has both mean and curl components.

6. Discussion

The previous section suggests that we may classify regimes of wind stress curl, horizontal circulation, and pumping velocity as follows: Regime 1 ($w_{E0} = 2T/f > 0$)—cyclonic circulation with upwelling due to Ekman

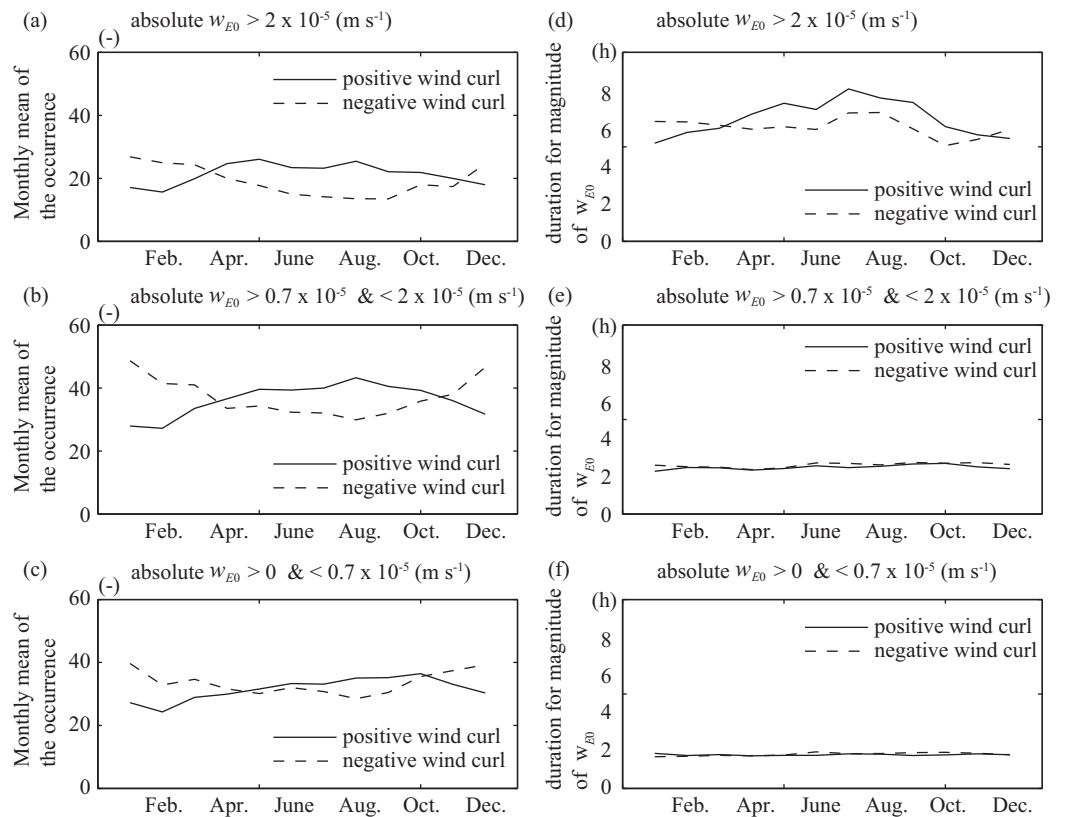


Figure 12. (left) Monthly mean of the occurrence and (right) duration for magnitude of w_{E0} (a and d) $> 0 \text{ m s}^{-1}$ and $< 0.7 \times 10^{-5} \text{ m s}^{-1}$, (b and e) $> 0.7 \times 10^{-5} \text{ m s}^{-1}$ and $< 2 \times 10^{-5} \text{ m s}^{-1}$, and (c and f) $> 2 \times 10^{-5} \text{ m s}^{-1}$.

and nonlinear pumping; Regime 2 ($-0.7 \times 10^{-5} \text{ m s}^{-2} < w_{E0} = 2T/f < 0$)—anticyclonic circulation with downwelling due to Ekman pumping; and Regime 3 ($w_{E0} = 2T/f < -0.7 \times 10^{-5} \text{ m s}^{-2}$)—anticyclonic circulation with conditional upwelling due to nonlinear pumping (Figure 10). In Regime 3, upwelling is conditional because it requires wind forcing with a long duration (Figure 7a). Note that the threshold between Regimes 2 and 3 may be specific to Tokyo Bay because the threshold was obtained from numerical simulations that included the effects of a lateral boundary. However, we expect that the threshold has a relatively small dependence on the lateral boundary, since the self-similar solution to the von Kármán swirling flow problem for infinite domains is applicable to the central part of the vortex in the presence of a lateral boundary [Rogers and Lance, 1964].

We used the above regimes to analyze the statistics of the direction of horizontal circulation and the sign of pumping velocity around the head of Tokyo Bay. To do this, we calculated the statistics of monthly mean w_{E0} from 1981 to 2004 (Figure 11). Monthly mean w_{E0} was found to be in Regime 1 from April to October and in Regime 2 from November to March, which suggests the likelihood that anticyclonic and cyclonic horizontal circulations appear around the head of Tokyo Bay during winter and summer, respectively. w_{E0} less than $0.7 \times 10^{-5} \text{ m s}^{-1}$, which corresponds to the threshold between Regime 2 and Regime 3, was found to occur 30 times in a month with typical duration of about 2 h (Figure 12). The duration of wind events with a w_{E0} magnitude larger than $2 \times 10^{-5} \text{ m s}^{-1}$ was about 6 h and was still shorter than the inertial period, suggesting that the Ekman pumping is dominant compared to nonlinear pumping (Figure 7a).

The strongly nonlinear Ekman layer investigated in this study is relevant to small to medium-sized lakes and bays surrounded by complex terrain. For example, typical wind stress curl over Lake Kinneret, Clear Lake, and Lake Biwa is $O(10^{-6} \text{ N m}^{-3})$ [Pan *et al.*, 2002; Rueda *et al.*, 2005; Shimizu *et al.*, 2007; Akitomo *et al.*, 2009]. This yields $w_{E0} = O(10^{-5} \text{ m s}^{-1})$, so the Ekman layer can be strongly nonlinear. If the wind duration is comparable or long compared to the inertial period, strong nonlinearity preferentially excites cyclonic circulation because the nonlinearity tends to induce cyclonic circulation below the Ekman layer. This could be one of the reasons why horizontal circulation tends to be cyclonic in lakes and semienclosed bays [Emery and Csanady, 1973]. On the other hand, typical wind stress curl over large lakes and the open ocean is $O(10^{-7} \text{ N m}^{-3})$ [Schwab and Beletsky, 2003; Riesen and Chelton, 2008], so $w_{E0} = O(10^{-6} \text{ m s}^{-1})$ at midlatitudes. Therefore, the Ekman layer remains approximately linear or only weakly nonlinear.

The results of this study suggest that particulate organic matter (POM) could be transported to the center of the bay head by the residual circulation driven by pumping velocity. Okada *et al.* [2009] carried out a field experiment to measure moisture content of the sediment from 2003 to 2004 using Quester tangent [Co., QTC VIEW; Preston *et al.*, 1999, Preston and Collins, 2000; Tsemahman and Collins, 1997]. These measurements were verified by comparison with sediment samples, and the field study demonstrated that sediment with a higher moisture content exists at the center of the bay head. In Tokyo Bay, higher moisture content corresponds to smaller sediment particles, which predominantly consist of POM [Okada *et al.*, 2009]. Therefore, areas of high moisture content indicate heavy accumulation of POM. In Tokyo Bay, water column POM is largely produced from June to September when red tides appear [Nakayama, 2005], coinciding with the time when upwelling occurs due to positive wind curl (Figures 10 and 11). Since POM tends to accumulate adjacent to the density interface and upwelling induces convergent flow immediately below the mixed layer, upwelling would result in accumulation of POM in the center of the gyre. Positive wind curl could be one of the primary factors controlling the accumulation of POM in the center of the bay head.

7. Conclusions

The results of three field experiments suggested that the deepening of isopycnals around the head of Tokyo Bay was induced by negative wind stress curl. Numerical simulations successfully reproduced the observed deepening, and showed that the deepening of the isopycnals and associated anticyclonic horizontal circulation are induced mainly by wind stress curl. The effects of river discharge induced noticeable changes in horizontal circulation, but those of surface heat fluxes and tides were very small. Theoretical and numerical solutions of steady nonlinear surface Ekman layers under uniform wind stress curl revealed that pumping velocities at the base of the surface mixed layer became positive under strongly negative wind stress curl, as the centrifugal force dominated the Coriolis force. We proposed to categorize the regimes of nonlinear surface Ekman layers as follows: Regime 1 ($w_{E0} = 2T/f > 0$)—upwelling due to Ekman and

nonlinear pumping; Regime 2 ($-0.7 \times 10^{-4} \text{ m s}^{-2} < w_{E0} = 2T/f < 0$)—downwelling due to negative Ekman pumping; and Regime 3 ($w_{E0} = 2T/f < -0.7 \times 10^{-4} \text{ m s}^{-2}$)—conditional upwelling due to nonlinear pumping. Wind statistics over Tokyo Bay suggests that Regimes 1 and 2 are most common in May to October and December to March, respectively. Regime 3 can occur under strong wind events in winter, but the typical duration of such events is not long enough to induce upwelling. We expect that convergent and divergent horizontal residual circulations immediately below the surface mixed layer are important for mass transport of POM in Tokyo Bay.

Acknowledgments

The authors thank Tomoyuki Kasuya and Keita Furukawa for helpful comments and an anonymous reviewer for their constructive comments, which have contributed to a significant improvement for this paper. This work has been supported by the Japan Society for the Promotion of Science. K.S. appreciates the financial support from the Max Planck Society for the Advancement of Science through the Klaus Hasselmann Postdoctoral Fellowship.

References

- Akitomo, K., K. Tanaka, M. Kumagai, and C. Jiao (2009), Annual cycle of circulations in Lake Biwa, part 2: Mechanisms, *Limnology*, *10*, 119–129.
- Benton, G. S., F. B. Lipps, and S. Y. Tuann (1964), The structure of the Ekman layer for geostrophic flows with lateral shear, *Tellus*, *16*, 186–199.
- Brink, K. H. (1997), Time-dependent motions and the nonlinear bottom Ekman layer, *J. Mar. Res.*, *55*, 613–631.
- Emery, K. O., and G. T. Csanady (1973), Surface circulation of lakes and nearly land-locked seas, *Proc. Natl. Acad. Sci. U. S. A.*, *70*, 93–97.
- Endoh, S. (1986), Diagnostic study on the vertical circulation and the maintenance mechanisms of the cyclonic gyre in Lake Biwa, *J. Geophys. Res.*, *91*, 869–876.
- Fujiwara, T. (2003), Buoyancy-driven current during cooling periods in Ise Bay, Japan, *J. Geophys. Res.*, *108*(C8), 3276, doi:10.1029/2002JC001521.
- Fujiwara, T., L. P. Sanford, K. Nakatsuji, and Y. Sugiyama (1997), Anti-cyclonic circulation driven by the estuarine circulation in a gulf type ROFI, *J. Mar. Syst.*, *12*, 83–99.
- Gill, A. E. (1982), *Atmosphere-Ocean Dynamics*, Academic, San Diego, Calif.
- Greenspan, H. P. (1968), *Theory of Rotating Fluids*, 327 pp., Cambridge Univ. Press, Cambridge, U. K.
- Guo, X., and T. Yanagi (1996), Seasonal variations of residual current in Tokyo Bay, Japan, *J. Oceanogr.*, *52*, 597–616.
- Guo, X., and T. Yanagi (1998), Variation of residual current in Tokyo Bay due to increase of fresh water discharge, *Cont. Shelf Res.*, *18*, 677–693.
- Hart, J. E. (2000), A note on nonlinear corrections to the Ekman layer pumping velocity, *Phys. Fluids*, *12*, 131–135.
- Horiguchi, F., and K. Nakata (1995), Water quality analysis of Tokyo Bay using mathematical model, *J. Adv. Mar. Sci. Technol.*, *1*, 71–92.
- Kasuya, T., M. Hamaguchi, and K. Furukawa (2004), Detailed observation of spatial abundance of clam larva *Ruditapes philippinarum* in Tokyo Bay, Central Japan, *J. Oceanogr.*, *60*, 631–636.
- Kondo, J. (1975), Air-sea bulk transfer coefficients in diabatic conditions, *Boundary Layer Meteorol.*, *9*, 91–112.
- Laval, B., J. Imberger, B. R. Hodges, and R. Stocker (2003), Modeling circulation in lakes: Spatial and temporal variations, *Limnol. Oceanogr. Methods*, *48*(3), 983–994.
- Leonard, B. P. (1991), The ULTIMATE conservative difference scheme applied to unsteady one-dimensional advection, *Comput. Methods Appl. Mech. Eng.*, *88*, 17–74, doi:10.1016/0045-7825(91)90232-U.
- Maruya, Y., K. Nakayama, T. Shintani, and M. Yonemoto (2010), Evaluation of entrainment velocity induced by wind stress in a two-layer system, *Hydrol. Res. Lett.*, *4*, 70–74, doi:10.3178/hrl.4.70.
- Matsumoto, E., and Y. Saito (1984), Environmental changes of Tokyo Bay by man in comparison with environmental changes by nature during geological history, *Bull. Geo. Surv. Japan*, *35*(6), 243–260.
- Nakamoto, A., K. Nakayama, T. Shintani, Y. Maruya, K. Komai, T. Ishida, and Y. Makiguchi (2013), Adaptive management in Kushiro Wetland in the context of salt wedge intrusion due to sea level rise, *Hydrol. Res. Lett.*, *7*(1), 1–5.
- Nakayama, K. (2005), Circulation processes in Tokyo Bay, in *The Environment in Asia Pacific Harbors*, edited by E. Wolanski, pp. 47–66, Springer, Singapore.
- Nakayama, K. (2006), Comparisons of using CIP, compact and CIP-CSL2 schemes for internal solitary waves, *Int. J. Numer. Methods Fluids*, *51*, 197–219.
- Nakayama, K., and J. Imberger (2010), Residual circulation due to internal waves shoaling on a slope, *Limnol. Oceanogr. Methods*, *55*, 1009–1023, doi:10.4319/lo.2010.55.3.1009.
- Nakayama, K., T. Okada, and M. Nomura (2005), Mechanism responsible for fortnightly modulations in estuary circulation in Tokyo Bay, *Estuarine Coastal Shelf Sci.*, *64*, 459–466.
- Nakayama, K., M. Sivapalan, C. Sato, and K. Furukawa (2010), Stochastic characterization of the onset of and recovery from Anoxia in Tokyo Bay, Japan: Derived distribution analysis based on “Strong Wind” events, *Water Resour. Res.*, *46*, W12532, doi:10.1029/2009WR008900.
- Nakayama, K., T. Shintani, K. Kokubo, Y. Maruya, T. Kakinuma, K. Komai, and T. Okada (2012), Residual current over a uniform slope due to breaking of internal waves in a two-layer system, *J. Geophys. Res.*, *117*, C10002, doi:10.1029/2012JC008155.
- Okada, T., P. Larcombe, and C. Mason (2009), Estimation of the spatial distribution of dredged material disposed of at sea by using particle-size distributions and metal concentrations, *Mar. Pollut. Bull.*, *58*, 1164–1177.
- Okada, T., K. Nakayama, T. Takao, and K. Furukawa (2011), Influence of freshwater input and bay reclamation on long-term changes in sea-water residence times in Tokyo Bay, Japan, *Hydrol. Processes*, *25*, 2694–2702, doi:10.1002/hyp.8010.
- Orlandi, P. (2000), *Fluid Flow Phenomena: A Numerical Toolkit*, Kluwer Acad., Netherlands.
- Pan, H., R. Avissar, and D. B. Haidvogel (2002), Summer circulation and temperature structure of Lake Kinneret, *J. Phys. Oceanogr.*, *32*, 295–313.
- Pedlosky, J. (1979), *Geophysical Fluid Dynamics*, Springer, Verlag.
- Pedlosky, J. (2008), On the weakly nonlinear Ekman layer: Thickness and flux, *J. Phys. Oceanogr.*, *38*, 1334–1339.
- Preston, J. M., and W. T. Collins (2000), Bottom classification in very shallow water by high-speed data acquisition, *OCEANS 2000 MTS/IEEE Conference and Exhibition*, *2*, 1277–1282, doi:10.1109/OCEANS.2000.881778.
- Preston, J. M., W. T. Collins, D. C. Mosher, R. H. Poekert, and R. H. Kuwahara (1999), The strength of correlations between geotechnical variables and acoustic classifications, *OCEANS'99 MTS/IEEE. Riding the Crest into the 21st Century*, *3*, 1123–1128, doi:10.1109/OCEANS.1999.800147.
- Riesen, C. M., and D. B. Chelton (2008), A global climatology of surface wind and wind stress fields from eight years of QuikSCAT scatterometer data, *J. Phys. Oceanogr.*, *38*, 2379–2413.
- Rogers, M. H., and G. N. Lance (1960), The rotationally symmetric flow of a viscous fluid in the presence of an infinite rotating disk, *J. Fluid Mech.*, *7*, 617–631.

- Rogers, M. H., and G. N. Lance (1964), The boundary layer on a disc of finite radius in a rotating fluid, *Q. J. Mech. Appl. Math.*, *17*, 319–330.
- Rueda, F. J., G. Schladow, S. G. Monismith, and M. T. Stacey (2005), On the effects of topography on wind and the generation of currents in a large multi-basin lake, *Hydrobiologia*, *532*, 139–151.
- Satoh, C., K. Nakayama, and K. Furukawa (2012), Contributions of wind and river effects on recovery of dissolved oxygen concentration in Tokyo Bay, *Estuarine Coastal Shelf Sci.*, *109*, 91–97, doi:10.1016/j.ecss.2012.05.023.
- Schwab, D. J., and D. Beletsky (2003), Relative effects of wind stress curl, topography, and stratification on large-scale circulation in Lake Michigan, *J. Geophys. Res.*, *108*(C2), 3044, doi:10.1029/2001JC001066.
- Shimizu, K., J. Imberger, and M. Kumagai (2007), Horizontal structure and excitation of primary motions in a strongly stratified lake, *Limnol. Oceanogr. Methods*, *52*, 2641–2655.
- Simanjuntak, M. A., J. Imberger, and K. Nakayama (2009), Numerical wave drag due to stair-step topography in a geophysical flow model, *J. Geophys. Res.*, *114*, C12020, doi:10.1029/2008JC005051.
- Suginohara, N. (1974), Onset of coastal upwelling in a two-layer ocean by wind stress with longshore variation [in Japanese with English abstract and captions], *Umi-no-Kenkyu*, *30*, 23–30.
- Suzuki, T., and M. Matsuyama (2000), Numerical experiments on stratified wind-induced circulation in Tokyo Bay, Japan, *Estuarine Coastal Shelf Sci.*, *50*, 17–25.
- Stern, M. E. (1965), Interaction of a uniform wind stress curl with a geostrophic vortex, *Deep Sea Res. Oceanogr. Abstr.*, *12*, 355–367.
- Tanaka, M. (2001), Numerical simulation for ecological system in enclosed bay [in Japanese with English abstract and captions], *Jpn. J. Nagare*, *20*, 354–364.
- Thomas, L. N., and P. B. Rhines (2002), Nonlinear stratified spin-up, *J. Fluid Mech.*, *473*, 211–244.
- Tsemahman, A. S., and W. T. Collins (1997), Acoustic seabed classification and correlation analysis of sediment properties by QTC View, *MTS/IEEE Conference OCEANS'97*, *2*, 921–926, doi:10.1109/OCEANS.1997.624114.
- Zandbergen, P. J., and D. Dijkstra (1987), Von Kármán swirling flows, *Annu. Rev. Fluid Mech.*, *19*, 465–491.
- Zavatarelli, M., N. Pinardi, V. H. Kourafalou, and A. Maggiore (2002), Diagnostic and prognostic model studies of the Adriatic Sea general circulation: Seasonal variability, *J. Geophys. Res.*, *107*(C1), 2–1–2–20, doi:10.0148-0227/02/2000JC000210.